1999년도 한국음향학회 학술발표대회 논문집 제18권 제2(s)호

결합형 유한요소-경계요소 기법에 의한 심해저용 30 kHz 전방향성 소나 변환기 최적 설계

장순석*, 최현호**, 이제형***, 안흥구***

조선대학교 전기.제어계측공학부*, 조선대학교 제어계측공학과**, 조선대학교 대학원 제어계측공학과***

Optimal Design of Deep-water 30 kHz Omnidirectional Sonar Transducer using a Coupled FE-BEM

Soon Suck Jarng, Heun Ho Choi, Je Hyeong Lee, Heung Gu Ahn

Dept. of Electrical Control & Instrumentation, Chosun University

Abstract

Deep-water sonar transducers of FFR (Free Flooded Ring) type have been designed using a coupled FE-BEM. The proposed sonar transducers are composed of piezoelectric ceramic tubes and structural steel materials for simple fabrication. In order to have an omnidirectional beam pattern around 30 kHz, a conic steel is placed below a piezoelectric tube or a steel disc is placed between two piezoelectric tubes. The dynamics of the sonar transducer is modelled in three dimensions and is analyzed with external electrical excitation conditions. Various results are available such as directivity patterns and transmitting voltage responses. The most optimal structure and dimensions of the steel material were calculated, so that the beam patterns of the sonar transducers had +/- 3 dB omnidirectivity at 30 kHz.

1. Introduction

This paper deals with the structural design of deep-water omnidirectional sonar transducers operating around 30 kHz. At 30 kHz of the mid-frequency band in, underwater sonar applications, the structural design of a sonar transducer must consider not only the dimensions of the piezoelectric ceramic but also the dimensions of any adjacent structural materials in order to produce omnidirectional directivity patterns. That is, the acoustic pressure field formed by the mutual interaction between the piezoelectric ceramic and the adjacent backing object produces different directivity patterns as the shape and the dimensions of the backing object are changed. Because of this mutual interaction of the acoustic pressure field the importance of the optimal design of the backing object increases. The optimal design of the sonar transducer is followed by the acousto-mechano-electrical simulation of the dynamic behaviour of the sonar transducer under the water.

A sonar transducer converts electric currents applied onto two electrodes of a piezoelectric material to the mechanical deformation of the piezoelectric ceramic which is radiated into an infinite fluid domain in the form of the acoustic pressure. The sonar transducer can be modelled by a coupled finite element-boundary element method (FE-BEM) [1,2]. The structural dynamics of the composite solid material can be modelled by the FEM, and coupling with the inviscid and compressive fluid material can be modelled by the BEM. The resulting coupled FE-BEM can simulate the infinite radiation of the acoustic pressure generated by the piezoelectric solid material in the fluid media. The infinite element method (IEM) is also applicable for the infinite radiation condition of the pressure sound at the outer boundary of the finite fluid domain [3]. Others use extra damping elements at the outer boundary of the finite fluid domain for the infinite radiation condition [4]. However these methods require too many fluid elements as an input frequency is increased. Also it is always difficult to generate fluid element meshes surrounding solid element meshes. The coupled FE-BEM need to generate no fluid elements.

The main aim of this paper is to optimally design deep-water 30 kHz sonar transducers with

an omnidirectional beam pattern using the coupled FE-BEM. Two particular structural cases are suggested and studied

2. Numerical Method

2.1 Finite Element Method (FEM)

The following equation (1) is the integral formulation of the piezoelectric equations:

$$\{F\}+\{F_f\} = [K_{uu}]\{a\} + [K_{u\phi}]\{\phi\} - \omega^2[M]\{a\} + j\omega[R]\{a\} \quad (1)$$

$$-\{Q\} = [K_{\phi u}]\{a\} + [K_{\phi\phi}]\{\phi\}$$

The isoparametric formulation for 3-dimensional structural elements is well documented by Allik H. et. al. [5]. Each 3-dimensional finite element is composed of 20 quadratic nodes and each node has nodal displacement (a_x, a_y, a_z) and electric potential (ϕ) variables. In local coordinates the finite element has 6 surface planes ($\pm$xy, $\pm$yz, $\pm$zx) which may be exposed to external fluid environment. The exposed surface is used as a boundary element which is composed of 8 quadratic nodes.

2.2 Boundary Element Method (BEM)

For sinusoidal steady-state problems, the Helmholtz equation, $\nabla^2\Psi + k^2\Psi = 0$, represents the fluid mechanics. Ψ is the acoustic pressure with time variation, $e^{j\omega t}$, and $k(=\omega/c)$ is the wave number. In order to solve the Helmholtz equation in an infinite fluid media, a solution to the equation must not only satisfy structural surface boundary condition (BC), $\frac{\partial\Psi}{\partial n} = \rho_f \omega^2 a_n$, but also the radiation condition at infinity, $\lim_{|r|\to\infty}\oint_S(\frac{\partial\Psi}{\partial r}+jk\Psi)^2 dS = 0$. $\frac{\partial}{\partial n}$ represents differentiation along the outward normal to the boundary. ρ_f and a_n are the fluid density and the normal displacement on the structural surface. The Helmholtz integral equation derived from Green's second theorem provides such a solution for radiating pressure waves;

$$\oint_S\left(\Psi(q)\frac{\partial G_k(p,q)}{\partial n_q} - G_k(p,q)\frac{\partial\Psi(q)}{\partial n_q}\right)dS_q = \beta(p)\,\Psi(p) - \Psi_{inc}(p) \quad (2)$$

where $G_k(p,q) = \frac{e^{-jkr}}{4\pi r}$, $r=|p-q|$

p is any point in either the interior or the exterior and q is the surface point of integration. β(p) is the exterior solid angle at p. $\Psi_{inc}(p)$ is an incident acoustic pressure. The acoustic pressure for the i^{th} global node, $\Psi(p_i)$, is expressed in discrete form [6]: ($1 \le i \le ng$)

$$= \sum_{m=1}^{nt}\int_{S_m}\left(\Psi(q)\frac{\partial G(p_i,q)}{\partial n_q} - G(p_i,q)\frac{\partial\Psi(q)}{\partial n_q}\right)dS_q \quad (3a)$$
$$q\in S_m$$

$$\beta(p_i)\,\Psi(p_i) - \Psi_{inc}(p_i) \quad (3b)$$
$$= \oint_S\left(\Psi(q)\frac{\partial G_k(p_i,q)}{\partial n_q} - G_k(p_i,q)\frac{\partial\Psi(q)}{\partial n_q}\right)dS_q$$

$$= \sum_{m=1}^{nt}\int_{S_m}\left(\begin{array}{l}\sum_{j=1}^{8}N_j(q)\Psi_{m,j}\frac{\partial G(p_i,q)}{\partial n_q} - \\ G(p_i,q)\sum_{j=1}^{8}N_j(q)\frac{\partial\Psi_{m,j}}{\partial n_q}\end{array}\right)dS_q \quad (3c)$$

$$= \sum_{m=1}^{nt}\sum_{j=1}^{8}\left(\int_{S_m}N_j(q)\frac{\partial G(p_i,q)}{\partial n_q}dS_q\right)\Psi_{m,j} - \rho_f\omega^2\sum_{m=1}^{nt}\sum_{j=1}^{8}\left(\int_{S_m}N_j(q)G(p_i,q)n_q dS_q\right)a_{m,j} \quad (3d)$$

$$= \sum_{m=1}^{nt}\sum_{j=1}^{8}A^i_{m,j}\Psi_{m,j} - \rho_f\omega^2\sum_{m=1}^{nt}\sum_{j=1}^{8}B^i_{m,j}a_{m,j} \quad (3e)$$

where nt is the total number of surface elements and $a_{m,j}$ are three dimensional displacements. Equation (3b) is derived from equation (3a) by discretizing integral surface. And equation (3c) is derived from equation (3b) since an acoustic pressure on an integral surface is interpolated from adjacent 8 quadratic nodal acoustic pressures corresponding the integral surface. Then equation (3d) is derived from equation (3c) by swapping integral notations with summing notations. Finally the parentheses of equation (3d) is expressed by upper capital notations for simplicity. When equation (3e) is globally assembled, the discrete Helmholtz equation can be represented as

$$([A]-\beta[I])\{\Psi\} = +\rho_f\omega^2[B]\{a\} - \{\Psi_{inc}\} \quad (4)$$

where [A] and [B] are square matrices of (ng by ng) size. ng is the total number of surface nodes. When the impedance matrices of equation (4), [A] and [B], are computed, two types of singularity arise [7]. One is that the Green's function of the equation, $G_k(p_i,q)$, becomes infinite as q approaches to p_i. This problem is solved by mapping such rectangular local coordinates into triangular local coordinates and again into polar local coordinates [8]. The other is that at certain wave number the matrices become ill-conditioned. These wave number are corresponding to eigenvalues of the interior Dirichlet problem [9]. One approach to overcome the matrix singularity is that [A] and [B] of equation (4) are modified to provide a unique solution for the entire frequency range [10~13]. The modified matrix equation referred to as the modified Helmholtz gradient formulation (HGF) [13] is obtained by adding a multiple of an extra integral equation to equation (4).

$$([A]-\beta[I]\oplus\alpha[C])\{\Psi\} = +\rho_f\omega^2([B]\oplus\alpha[D])\{a\} - (\Psi_{inc}\oplus\alpha\frac{\partial\Psi_{inc}}{\partial n_p}) \quad (5)$$

where

$$\alpha = -\frac{\sqrt{-1}}{k\cdot\left(\begin{array}{c}Number\ of\ surface\ elements\\ adjacent\ a\ surface\ node\end{array}\right)}$$

[C] and [D] are rectangular matrices of (nt by ng) size. nt is the total number of surface elements. $\oplus$ symbol indicates that the rows of [C],[D] corresponding to surface elements adjacent

a surface node are added to the row of [A],[B] corresponding to the surface node, that is, (6)

$$\sum_{i=1}^{nt}\sum_{j=1}^{nt}A(i,j) = \sum_{i=1}^{nt}\sum_{j=1}^{nt}A(i,j) + \sum_{i=1}^{nt}\sum_{j=1}^{nt}\left(\sum_{m=1}^{S(i)} a\ C(m,j)\right)$$

$$\sum_{i=1}^{nt}\sum_{j=1}^{nt}B(i,j) = \sum_{i=1}^{nt}\sum_{j=1}^{nt}B(i,j) + \sum_{i=1}^{nt}\sum_{j=1}^{nt}\left(\sum_{m=1}^{S(i)} a\ D(m,j)\right)$$

where S(i) is the number of surface element adjacent a surface node. The derivation of the extra matrices [C],[D] are well described by Francis D.T.I.[13]. Equation (6) may be reduced in its formulation using superscript $\oplus$ for convenience;

$$A^{\oplus}\{\Psi\} = +\rho_f\,\omega^2 B^{\oplus}\{a\} - \Psi_{inc}^{\oplus} \quad (7)$$

Equation (7) can be written as

$$\{\Psi\} = +\rho_f\,\omega^2 (A^{\oplus})^{-1} B^{\oplus}\{a\} - (A^{\oplus})^{-1}\Psi_{inc}^{\oplus} \quad (8)$$

2.3 Coupled FE-BE Method

The acoustic fluid loading on the solid-fluid interface generates interaction forces. These forces can be related to the surface pressures by a coupling matrix [L] [6,14];

$$\{F_f\} = -[L]\{\ddot{\Psi}\} \quad (9)$$

where $[L] = \int N^t n N dS$. N is a matrix of surface shape functions and n is an outward normal vector at the surface element. N^t is the transposed form of N matrices. Equations (8) and (9) indicate that the interaction force can be expressed by functions of elastic displacement instead of acoustic pressure. This relationship can be applied to equation (1) when the sonar transducer model is submerged into the infinite fluid media: (10)

$$\{F\}+[L](A^{\oplus})^{-1}\Psi_{inc}^{\oplus} = [K_{uu}]\{a\}+[\rho_f\,\omega^2[L](A^{\oplus})^{-1}B^{\oplus}]$$

$$\{a\}+[K_{u\phi}]\{\phi\}\omega^2[M]\{a\}+j\omega[R]\{a\}$$

$$\{Q\} = [K_{\phi u}]\{a\}+[K_{\phi\phi}]\{\phi\}$$

where

$\Psi_{inc}^{\oplus}$ Incident Pressure

$[L]$ Coupling Matrix at the Fluid-Structure Interface

$A^{\oplus}$ Fluid BEM Matrix [A]

$B^{\oplus}$ Fluid BEM Matrix [B]

ρ_f Fluid Density, $j = \sqrt{-1}$

Since the present sonar transducer is modelled as a projector, the internal force vector, $\{F\}$, and the external incident pressure, $[L](A^{\oplus})^{-1}\Psi_{inc}^{\oplus}$, of equation (10) are removed. The only applied BC for the equation is the applied electrical charge vector, $\{Q\}$. The acoustic pressure in the far field is determined by $\beta(p)=1$ for given values of surface nodal pressure and surface nodal displacement;

$$\Psi(p_i) = \sum_{m=1}^{nt}\sum_{j=1}^{s} A'_{m,j}\Psi_{m,j} - \rho_f\,\omega^2\sum_{m=1}^{nt}\sum_{j=1}^{s} B'_{m,j}a_{m,j} - (A^{\oplus})^{-1}\Psi_{inc}^{\oplus} \quad (11)$$

2.4. Modelling of omnidirectional piezoelectric sonar transducers

Two particular structural designs are considered for omnidirectional sonar transducers. One is that a conic steel is placed below a piezoelectric tube (Figure 1). And the other is that a steel disc is placed between two piezoelectric tubes (Figure 2). A ceramic tube is the most common shape in deep-water sonar transducer design. Table 1 is the dimensions of the ceramic tube. The ceramic tube is polarized in radial axis.

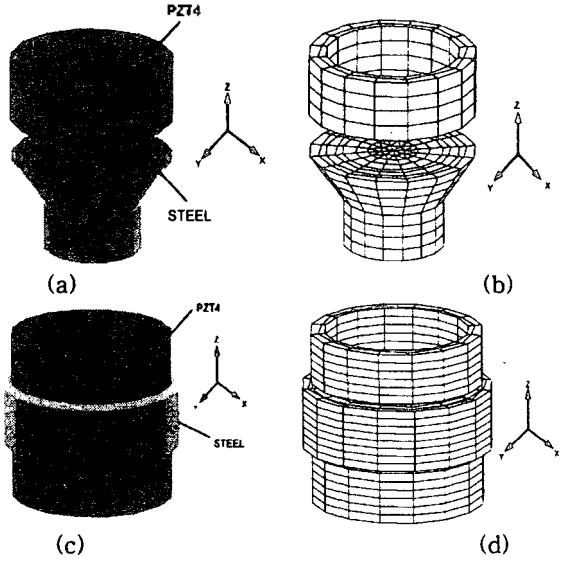

Figure 1 Three dimensional views of sonar transducers, (a) and (c), and their structural finite elements, (b) and (d).

Table 1 Dimensions of the ceramic tube

Type	[mm]
Inner Radius	31.98
Outer Radius	38.20
Height	12.70

Table 2 and Table 3 show property values of the materials used for the sonar transducer.

Table2.Piezoelectric Material Properties of PZT4 (Axially Polarized Properties)

No	Value	Unit	No	Value	Unit
ρ	7500	Kg/m^3	C_x^x	3.06E+10	N/m^2
C_x^x	1.39E+11	N/m^2	$e_{p_x}^x$	-5.2	N/Vm
C_y^x	7.78E+10	N/m^2	$e_{p_x}^y$	-5.2	N/Vm
C_z^x	7.43E+10	N/m^2	$e_{p_x}^z$	15.1	N/Vm
C_y^y	1.39E+11	N/m^2	$e_{p_x}^{yz}$	12.7	N/Vm
C_z^y	7.43E+10	N/m^2	$e_{p_x}^{zx}$	12.7	N/Vm
C_z^z	1.15E+11	N/m^2	ε_x^x	6.46E-9	F/m
C_y^y	2.56E+10	N/m^2	ε_y^y	6.46E-9	F/m
C_z^z	2.56E+10	N/m^2	ε_z^z	5.62E-9	F/m
K_{33}	0.69	-	K_{15}	0.70	-

Table 3 Properties of other materials used for the omnidirectional sonar transducer design

Property / Material	Density ρ [Kg/m^3]	Young's Modulus Y [N/m^2]	Poison's Ratio γ
Air	1.22	1.411E5	-
Water	1000	0.222E10	-
Steel	7850	207.0E9	029

3. Results and Discussions

The coupled FE-BE method has been programmed with Fortran language running at a SUN workstation. Calculation is done with double precision and the program is made for three dimensional structures. It is a common practice to have the size of the largest element to be less than $\lambda/3$.

3.1. One ceramic tube with a conic steel

The dimension of the conic steel was kept constant while the gap between the ceramic tube and the conic steel was changed to produce the best omnidirectional beam pattern. Figure 2 shows the directivity pattern of the sonar transducer at 30 kHz with 1mm gap. The ceramic tube is coated with non-conductive materials, and the ceramic and the mounting steel is moulded with a rubber which has the similar impedance as the water. The difference between the maximum acoustic pressure level and the minimum acoustic pressure level is defined as a directivity variation.

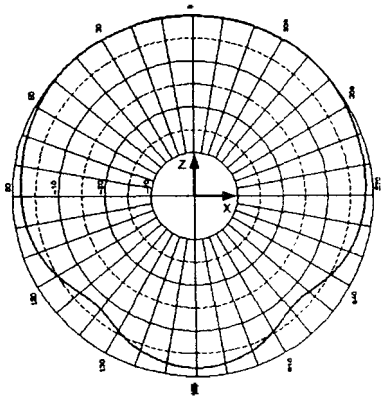

Figure 2 The directivity pattern of the sonar transducer at 30 kHz with 1mm gap.

Figure 3 shows the directivity variation as a function of the gap. At 9mm gap the sonar transducer results in the lowest directivity variation of 4.9 [dB]. Figure 4 shows the dimensional shape of the optimally designed sonar transducer. And figure 5 shows the directivity pattern for the optimally designed sonar transducer at 30 kHz.

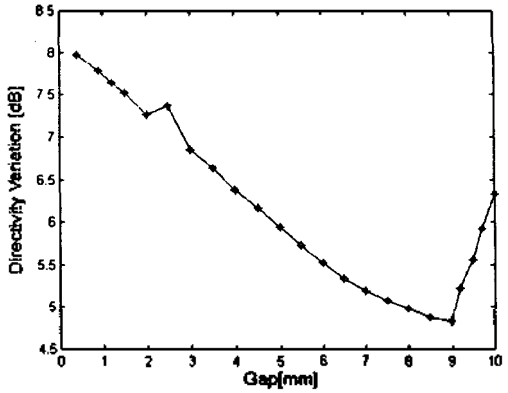

Figure 3 The directivity variation as a function of the gap

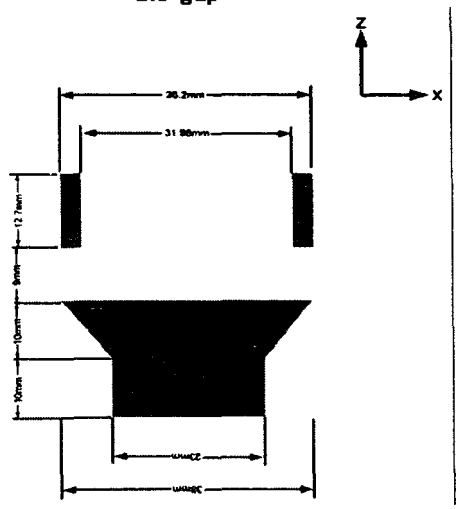

Figure 4 The dimensional shape of the optimally designed sonar transducer.

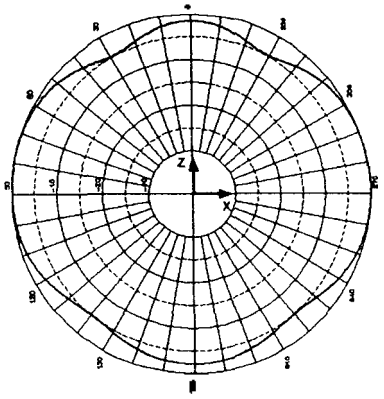

Figure 5 The directivity pattern of the sonar transducer at 30 kHz with 9mm gap.

Figure 6 shows the transmitting voltage responses (TVR) of the optimally designed sonar transducer. The TVR is calculated at 1m from the source origin. Three' labels in the figure indicate directions of TVR. The TVR shows +/- 3 dB frequency response between 20 kHz and 33 kHz in the Z axis. The sharp peak resonance in the figure is probably due to the adjacent elastic structure and the gap. And figure 7 shows the G-B graph of the sonar transducer.

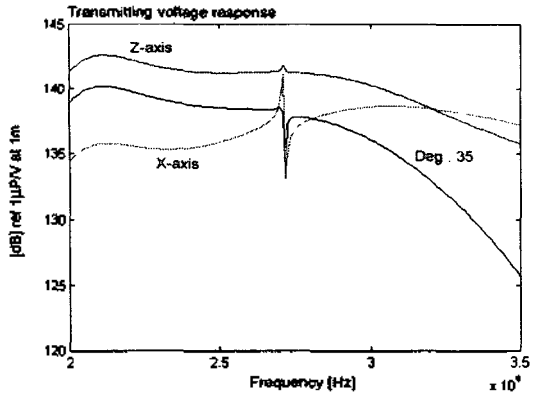

Figure 6 The TVR of the optimally designed sonar transducer.

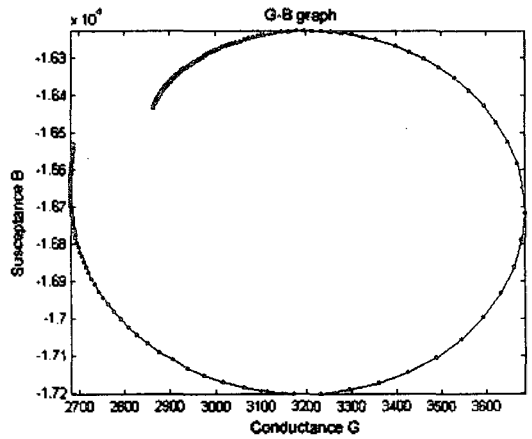

Figure 7 The G-B graph of the sonar transducer.

3.2. Two ceramic tubes and one steel disc

The dimensions of the steel disc were kept constant while the gap between the ceramic tubes and the steel disc was changed to produce the most omnidirectional beam pattern. The two ceramics are connected in the inner electrodes and the outer electrodes for electrical drive with the same phase. Figure 8 shows the directivity pattern of the sonar transducer at 30 kHz with 1mm gap which produces the lowest directivity variation, 5.3 [dB]. And figure 9 shows the dimensional shape of the optimally designed sonar transducer.

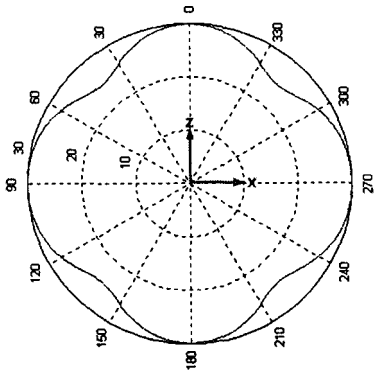

Figure 8 The directivity pattern of the sonar transducer at 30 kHz with 1mm gap.

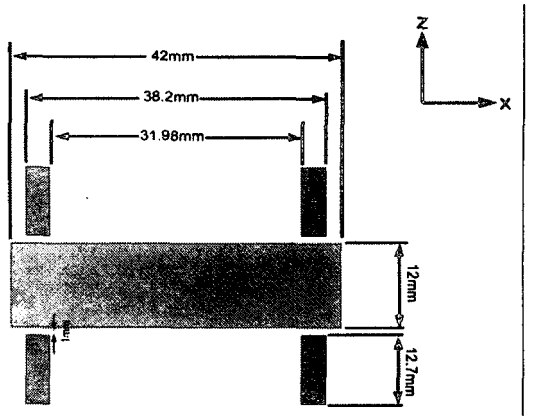

Figure 9 The dimensional shape of the optimally designed sonar transducer.

Figure 10 shows the TVR of the optimally designed sonar transducer. The TVR shows +/- 3 dB frequency response between 20 kHz and 35 kHz in the Z axis except at a resonance around 28 kHz. And figure 11 shows the G-B graph of the sonar transducer. It is noticed that the TVR of the ceramic tube above the conic steel has higher output acoustic power than that of the steel disc between two ceramic tubes. It is because the former transducer (the ceramic tube above the conic steel) has twice more capacitance than the latter transducer (the steel disc between two ceramic tubes).

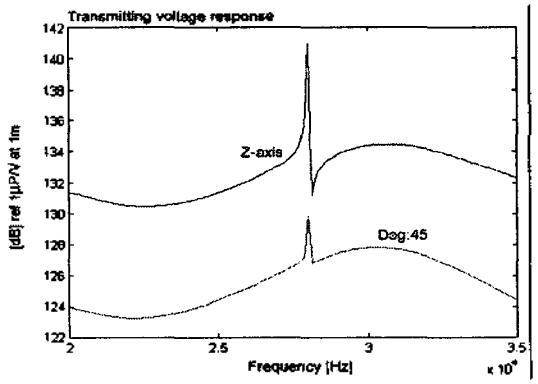

Figure 10 The TVR of the optimally designed sonar transducer.

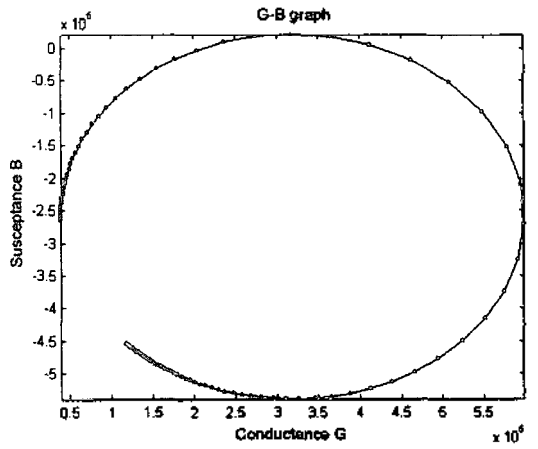

Figure 11 The G-B graph of the sonar transducer.

4. Conclusion

Deep-water sonar transducers of FFR type have been designed using a coupled FE-BEM. In order to have an omnidirectional beam pattern at 30 kHz, a conic steel is placed below a piezoelectric tube or a steel disc is placed between two piezoelectric tubes. The optimal structure and dimensions of the steel material are suggested, so that the beam patterns of the sonar transducers have +/- 3 dB omnidirectivity at 30 kHz. It is also concluded that the transducer with conic steel could be better in omnidirectional directivity than that with steel disc. In addition, TVR of the proposed transducers is analyzed and it is found that TVR is optimal in frequency range of interest.

ACKNOWLEDGEMENTS

This study was supported by a grant from STEPI (Science and Technology Policy Institute) Korea under contract I-03-020, as part of the 1998 international programme of collaboration between Korea and the United Kingdom and by a grant from the European Community under contract MAS3-CT95-0031 (BASS).

References

[1] S.S. Jarng, "SONAR Transducer Design & Optimization using the Finite Element Method", Ph.D. Thesis, University of Birmingham, Engineering Faculty, 1991.12.

[2] S.S. Jarng, "PZT5 shell-typed hydrophone simulation using a coupled FE-BE method", Proceedings Institute of Acoustics, Vol. 21, Pt.1, PP:51-60, 1999.4.

[3] J.P.E. Goransson and C.F. Davidsson, "A three dimensional infinite element for wave propagation", J. Sound & Vibration, Vol. 115(3), PP:558-559, 1987.

[4] R. Bossut and J.N. Decarpigny, "Finite element modeling of radiating structures using dipolar damping elements", J. Acoust. Soc. Am. Vol. 86, No. 4, PP:1234-1244, 1989.

[5] H. Allik and T.J.R. Hughes, "Finite element method for piezoelectric vibration", Int. J. Numer. Method Eng., Vol. 2, PP:151-157, 1970.

[6] L.G. Copley, "Integral equation method for radiation from vibrating bodies", J. Acoust. Soc. Am. Vol. 41, PP:807-816, 1967.

[7] L.G. Copley, "Fundamental results concerning integral representations in acoustic radiation", J. Acoust. Soc. Am. Vol. 44, PP:28-32, 1968.

[8] E. Skudrzyk, "The foundation of acoustics", (Springer-Verlag, New York, 1971), PP:408-409, Equation(76), 1971.

[9] D.T.I. Francis, "A boundary element method for the analysis of the acoustic field in three dimensional fluid-structure interaction problems", Proc. Inst. of Acoust., Vol. 12, Part 4, PP:76-84, 1990.

[10] H.A. Schenck, "Improved integral formulation for acoustic radiation problems", J. Acoust. Soc. Am. Vol. 44, PP:41-58, 1968.

[11] A.J. Burton and G.F. Miller, "The application of integral integration methods to the numerical solutions of some exterior boundary problems", Proc. R. Soc. London, Ser. A 323, PP:201-210, 1971.

[12] R.F. Kleinman and G.F. Roach, "Boundary integral equations for the three dimensional Helmholtz equation", SIAM Rev., Vol. 16, PP:214-236, 1974.

[13] D.T.I. Francis, "A gradient formulation of the Helmholtz integral equation for acoustic radiation and scattering", J. Acoust. Soc. Am. Vol. 93(4) Part 1, PP:1700-1709, 1993.

[14] O.C. Zienkiewicz, D. Kelly and P. Bettess, "The coupling of finite element method and boundary solutions procedures", Int. J. Num. Methods Eng., Vol. 11, PP:355-375, 1977.